THE ASTROPHYSICAL JOURNAL, 491:165–171, 1997 December 10

SMALL-SCALE VARIATIONS IN THE $\frac{1}{4}$ keV X-RAY BACKGROUND ALONG THE GALACTIC PLANE

SANGWOOK PARK AND JOHN P. FINLEY
Department of Physics, Purdue University, 1396 Physics Building, West Lafayette, IN 47907; parksan@purds1.physics.purdue.edu, finley@purds1.physics.purdue.edu

AND

S. L. SNOWDEN[1]
NASA Goddard Space Flight Center, Code 662, Greenbelt, MD 20771; snowden@lheavx.gsfc.nasa.gov
Received 1997 June 5; accepted 1997 July 24

ABSTRACT

Forty-two *ROSAT* Position Sensitive Proportional Counter pointed observations in the first quadrant ($l \sim 4°$–$26°$) of the Galactic plane are mosaicked in order to study the spatial structure of the X-ray–emitting gas in the Local Hot Bubble (LHB). X-ray intensity variations at various angular scales are examined in the $\frac{1}{4}$ keV band, and degree-scale variations are detected. In the context of the LHB and the displacement model for the origin of the $\frac{1}{4}$ keV band background, the hardness ratio, angular size, and magnitude of the intensity variations suggest that at the $\pm 10\%$ level there is an influence of a clumpy boundary structure superposed upon the emission from the uniformly distributed $\sim 10^6$ K plasma of the LHB interior. The possible origins of such a clumpy boundary structure of the LHB are discussed with Rayleigh-Taylor instabilities and clumping of the cooler interstellar medium at the boundary region being likely candidates.

Subject headings: diffuse radiation — ISM: bubbles — ISM: structure — X-rays: ISM

1. INTRODUCTION

The $\frac{1}{4}$ keV (0.1–0.3 keV) band diffuse X-ray background emission is most likely thermal (Williamson et al. 1974; McCammon & Sanders 1990) and is dominated by an $\sim 10^6$ K plasma contained in an extensive cavity in the Galactic disk (~ 100 pc in average extent), which contains the Sun. The first all-sky study of the $\frac{1}{4}$ keV X-ray background was performed by a University of Wisconsin group (McCammon et al. 1983). The most notable characteristic of the Wisconsin survey in the $\frac{1}{4}$ keV band (B and C bands) was the general anticorrelation between X-ray intensity and Galactic neutral hydrogen column density ($N_{\rm H}$) that had been noted over more limited regions since the $\frac{1}{4}$ keV background was first observed (Bowyer, Field, & Mack 1968). The observed anticorrelation was not thought to be caused entirely by photoelectric absorption by neutral interstellar material, for the following reasons: (1) the X-ray intensity variations are not energy dependent, (2) the effective absorption cross sections are too small, (3) residual flux in the Galactic plane exists, and (4) the $N_{\rm H}$ versus X-ray intensity relation has a large scatter (Sanders et al. 1977; McCammon et al. 1983; McCammon & Sanders 1990). In order to explain the observed anticorrelation between $N_{\rm H}$ and the X-ray intensity, Sanders et al. (1977) suggested a "displacement effect" that assumes the existence of a cavity around the solar system deficient in absorbing neutral material. Within the context of this model, the general anticorrelation between $N_{\rm H}$ and the observed X-ray intensity is explained by the respective path lengths through the X-ray–emitting plasma within the cavity and the H I beyond the cavity. An extension of the plasma that increases the $\frac{1}{4}$ keV intensity "displaces" H I and reduces the H I column density, providing the observed anticorrelation. Observational support for the H I cavity comes from 21 cm $N_{\rm H}$ measurements (Knapp 1975) and optical interstellar medium (ISM) absorption-line studies (Frisch & York 1983; Paresce 1984). Theoretical support for the existence of a local hot cavity was put forth by Cox & Anderson (1982). Their work demonstrated that the observed $\frac{1}{4}$ keV band X-ray intensity can be reproduced by a blast wave of energy 3×10^{50} ergs propagating through an ISM of density 0.004 cm^{-3}. The required model radius of the cavity is ~ 100 pc. Currently, the most widely accepted explanation of the $\frac{1}{4}$ keV band diffuse X-ray background is the emission from a rarefied $\sim 10^6$ K gas within this cavity, the so-called Local Hot Bubble (LHB; Cox & Reynolds 1987), with a contribution from a Galactic X-ray halo at higher Galactic latitudes (Snowden et al. 1997). The inferred radius of the LHB ranges from about 40 to 90 pc along the Galactic plane and up to ~ 130 pc at higher latitudes. The estimated average $N_{\rm H}$ within the LHB is less than 5×10^{18} cm^{-2} (Bloch et al. 1986; Juda et al. 1991). At low Galactic latitudes, model emission from the LHB satisfies the general observational characteristics of the $\frac{1}{4}$ keV background and provides essentially all of the observed flux exclusive of a limited number of discrete emission features (supernova remnants and possibly stellar wind bubbles).

In the Galactic plane, the $\frac{1}{4}$ keV band diffuse emission (exclusive of discrete emission features) is expected to originate within the LHB because of the substantial optical depth of the ISM. This "isolation" from the contribution of a flux of distant Galactic origin allows the study of the detailed structure of the LHB. The current LHB model assumes a uniform distribution of the X-ray–emitting gas inside the bubble. Models for an interstellar bubble, however, predict the formation of a dense boundary shell. If this is the case, a substantial contribution to the emission due to the boundary structure in the $\frac{1}{4}$ keV background could be expected (e.g., Slavin & Cox 1992). The detailed structure of the X-ray–emitting gas of the LHB can therefore be studied by searching for X-ray intensity variations in the $\frac{1}{4}$ keV band at different angular scales. Small angular

[1] Universities Space Research Association.

scale (less than a few degrees) X-ray intensity variations are not likely to be caused by the displacement effect associated with the general expansion of the LHB, which is linked to larger-scale ($\gtrsim 30°$) variations. Instead, they might probably arise from a contribution from a relatively thin emission region such as a boundary layer. Here we report a detection of degree-scale diffuse X-ray intensity variations in the first quadrant ($l \sim 4°$–$26°$) of the Galactic plane. The most prominent scale size is $\sim 5.°5$. This result implies a significant influence by a shell-like boundary structure of the LHB on the observed $\frac{1}{4}$ keV band diffuse X-ray background. The data used in this study are described in § 2. The results and implications are discussed in §§ 3 and 4. A summary is presented in § 5.

2. DATA

Over 20° ($l \sim 4°$–$26°$) of the Galactic plane is continuously covered (except for a 2° "gap" at $l \sim 15°$) by 42 *ROSAT* Position Sensitive Proportional Counter (PSPC) pointed observations. All of these 42 observations are in the public domain and have been obtained through the HEASARC *ROSAT* archive. All identified noncosmic backgrounds (i.e., the particle background, scattered solar X-ray background, long-term enhancements, and the afterpulse background) are modeled and subtracted from the data, following the methods described by Snowden et al. (1994) and references therein. Contamination due to short-term enhancements, such as auroral X-rays, solar flares, and enhanced charged-particle rates encountered near the South Atlantic Anomaly and particle belts, is removed by excluding all observational time intervals that display anomalous peaks in their light curves. For the observations used in this study, the average modeled noncosmic background is ~22% of the total counts in the $\frac{1}{4}$ keV band. After all the modeled noncosmic backgrounds and detected point sources are removed, the individual pointings are merged into large-area mosaics. Possible emission features due to extended discrete sources (e.g., supernova remnants) were also removed from the individual observations. The removed point and extended sources are listed in Table 1. The relative offsets in the zero level between the individual observations are determined by simultaneously comparing the average count rates in overlapping regions between all pairs of observations. The contribution from this correction is ~9% on average. The $\frac{1}{4}$ keV band mosaic is divided into two subbands: the R1L (0.11–0.284 keV) band and the R2 (0.14–0.284 keV) band (band definitions and band response functions can be found in Snowden et al. 1994). The large spectral overlap between the two subbands is due to the poor spectral resolution of the PSPC in this energy range ($E/\Delta E \sim 1$).

TABLE 1

REGIONS EXCLUDED IN THE ANALYSIS BECAUSE OF POSSIBLE CONTAMINATION BY DISCRETE EMISSION FEATURE

Name	l (deg)	b (deg)	Type
W28	6.5	−0.1	SNR
G7.4−1.4	7.4	−1.4	SNR (?)
G11.2−0.3	11.2	−0.3	SNR
GRS 1758−258	4.5	−1.4	XRB
G18.95−1.1	18.9	−1.1	SNR
GX 17+2	16.4	1.4	LMXRB
GX 5−1	5.1	−1.0	LMXRB
GX 9+1	9.1	+1.2	LMXRB

The final mosaic of the 42 *ROSAT* PSPC pointed observations is displayed in Figure 1. For the figure, the data were binned into 10′ pixels and smoothed; unsmoothed 10′ pixels were used for the analysis. As a mosaic, the data cover ~60 deg^2 along the Galactic plane with an average exposure of ~8 ks. This average exposure together with the 10′ binning yields an average of 9%, 8%, and 6% statistical error for the individual pixels in the R1L, R2, and R1L+R2 bands, respectively. The difference of the average count rates between the two separate regions in Figure 1 is small and therefore produces no significant influence when combined as a mosaic. For example, the count rate difference between two regions in the R1L+R2 band is ~4%, which is within the average statistical uncertainty (~6% pixel^{-1}).

3. ANALYSIS AND RESULTS

The $\frac{1}{4}$ keV band X-ray intensity distribution is relatively

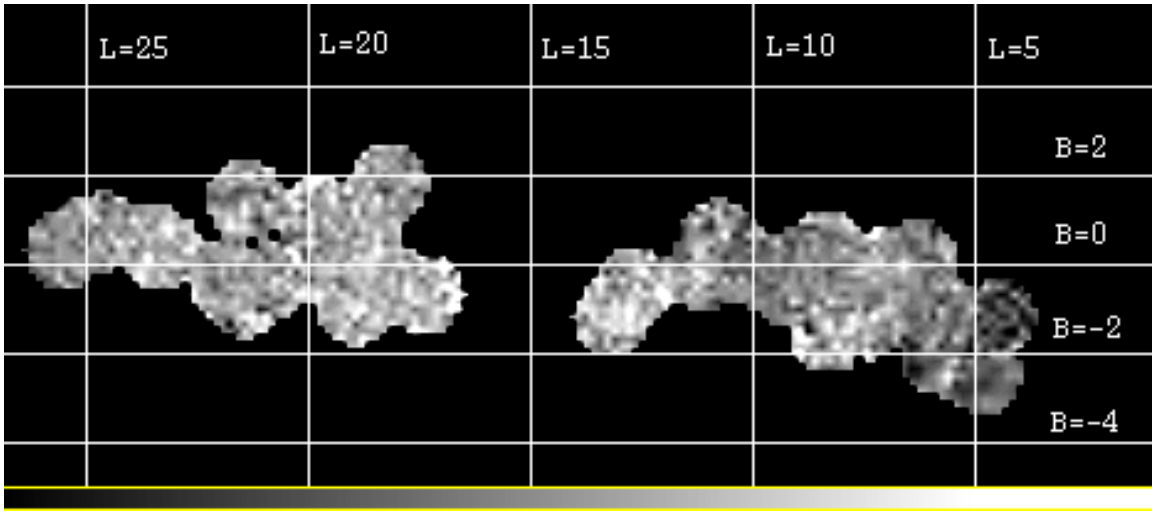

FIG. 1.—The $\frac{1}{4}$ keV band (R1L+R2) image of the Galactic plane from the mosaic of the 42 *ROSAT* PSPC pointed observations. The pixel size is 10′ and the data have been smoothed with an adaptive filtering algorithm by selecting an area that contains 100 counts. The gray scale ranges from zero to 800×10^{-6} counts s^{-1} arcmin^{-2}. The gap at $l \sim 14°$–$16°$ in the map is due to the exclusion of an observation that overlaps with no other pointings.

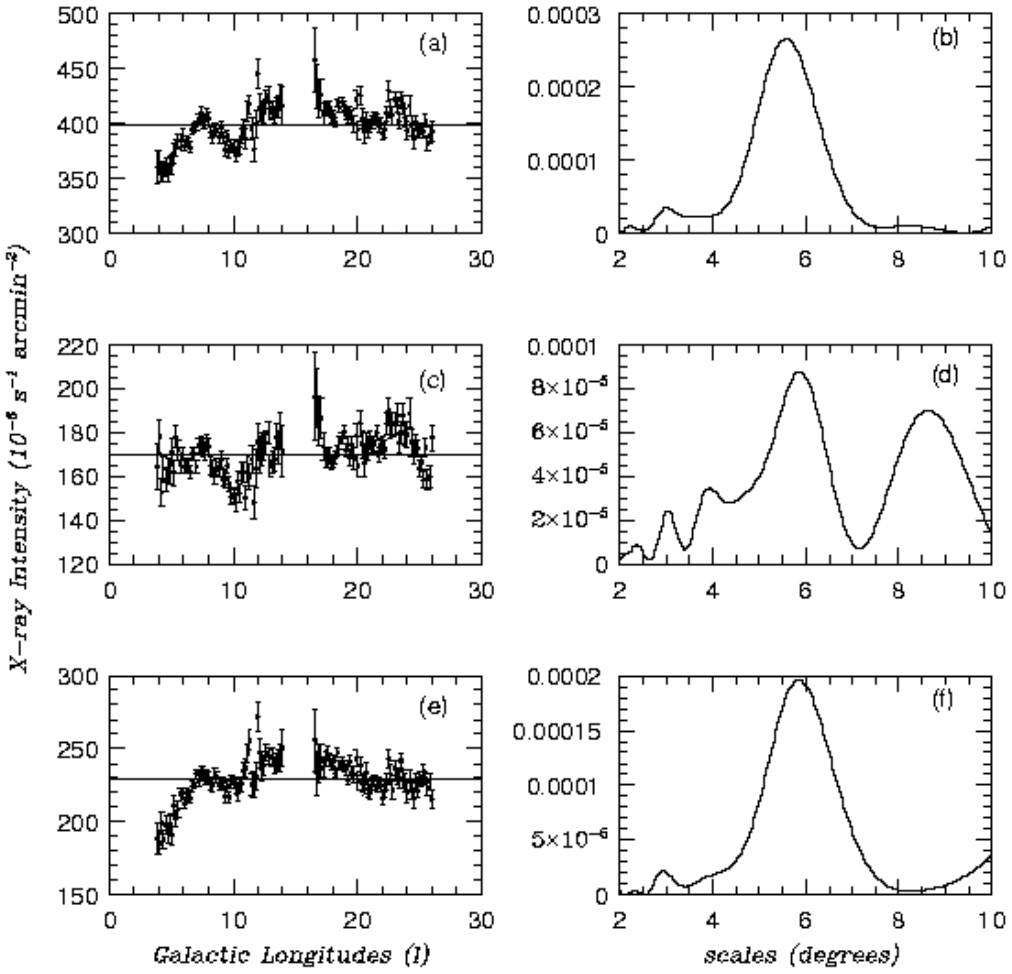

FIG. 2.—The $\frac{1}{4}$ keV band X-ray intensity variations along the Galactic plane. Each point corresponds to a 10′ column integrated across the Galactic plane ($b \sim -3.^{\circ}5$–2°). The horizontal lines represent the mean intensity. (*a*) R1L + R2 band intensity; (*b*) Fourier transform of (*a*). (*c*–*f*) X-ray intensity and spatial Fourier transform for the R1L and R2 subbands, respectively.

featureless (Fig. 1). This is expected in the context of the displacement model, in which nearly all the diffuse X-ray emission in the Galactic plane in this bandpass should originate within the LHB because of the short mean free path of the X-rays through the neutral material in the Galactic disk (e.g., ~ 30 pc in the $\frac{1}{4}$ keV band assuming $n_{\rm H} \sim 1$ cm^{-3}). In order to search for X-ray intensity variations along the Galactic plane, the data were first integrated across the plane in Galactic latitude b, typically within $\pm 2^{\circ}$ from the plane, for every 10′ along the Galactic longitude. While this binning (10′ × $\sim 3^{\circ}$ on average) may not be sensitive to sub–degree-scale variations due to the angular sampling across the plane, it is sufficiently sensitive to degree-scale variations that can still be indicative of the boundary structure of the LHB. The adopted one-dimensional binning also yields the best statistics ($\sim 2\%$ per bin on average) along the plane for the detection of small-magnitude intensity variations. The X-ray intensity variations along the Galactic plane are displayed in Figure 2. The average flux in the $\frac{1}{4}$ keV band (R1L + R2) is $\sim 400 \times 10^{-6}$ counts s^{-1} arcmin^{-2} (Fig. 2*a*), which is consistent with the *ROSAT* All-Sky Survey. For comparison, the $\frac{1}{4}$ keV band (R1 + R2) intensity of the *ROSAT* All-Sky Survey (Snowden et al. 1995) in the same region of the Galactic plane is displayed in Figure 3, where each bin is integrated across the plane with a 3° cut. The $\frac{1}{4}$ keV band of the *ROSAT* All-Sky Survey comprises the R1 and R2 bands (R12 band). The R1/R1L band ratio is ~ 1.2 (Snowden et al. 1994) for a thermal equilibrium model spectrum at $10^{6.1}$ K (Snowden et al. 1997). For the same model emission temperature, the R12/R1L2 band ratio is ~ 1.09. The difference between our data and the average

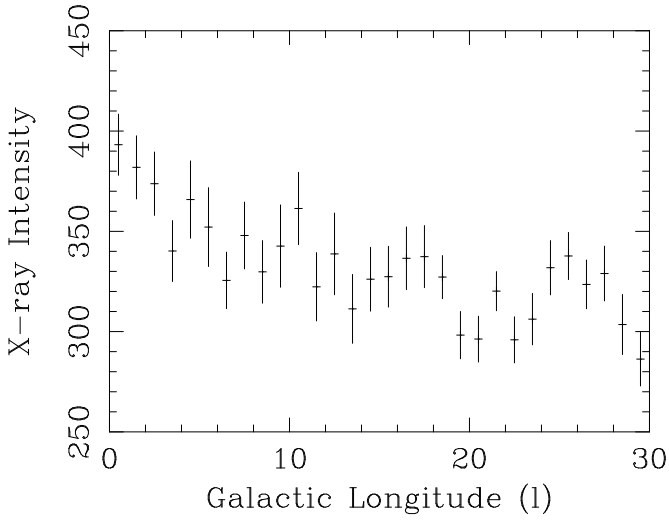

FIG. 3.—The $\frac{1}{4}$ keV band X-ray intensity along the Galactic plane from the *ROSAT* All-Sky Survey (Snowden et al. 1995).

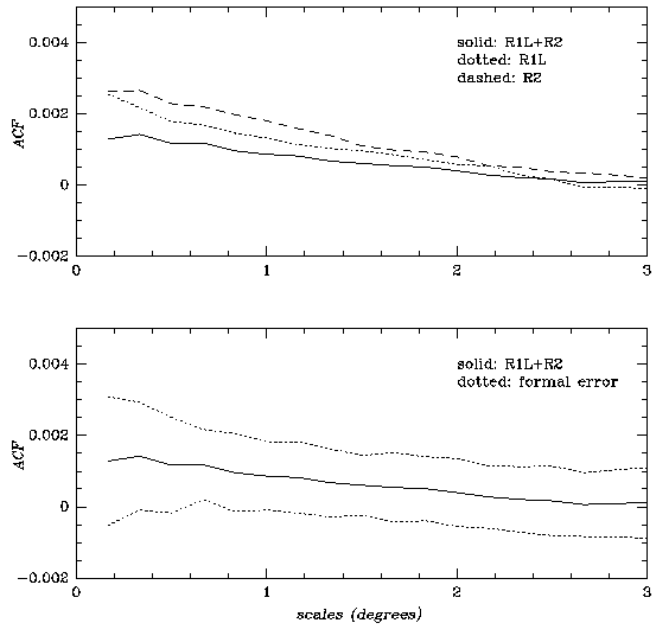

FIG. 4.—The ACF of the $\frac{1}{4}$ keV band X-ray intensity for angular scales $\leq 3°$. *Top*, ACFs for the R1L (*dotted line*), the R2 (*dashed line*), and the R1L + R2 (*solid line*) bands; *bottom*, R1L + R2 band ACF (*solid line*) and its formal uncertainty (*dotted lines*).

All-Sky Survey data ($\sim 340 \times 10^{-6}$ counts s^{-1} arcmin^{-2} in the R12 band or $\sim 315 \times 10^{-6}$ counts s^{-1} arcmin^{-2} in the R1L+R2 band) indicates a residual zero-level offset of $\sim 30\%$ in our mosaic. An offset in the count rates between the All-Sky Survey and the mosaic of the pointed observations is perhaps expected since individual *ROSAT* PSPC pointings cannot be cleansed of the nonvarying part of the long-term enhancements background component. A few inconsistent features are also observed, e.g., at $l \sim 4°$–$5°$, $l \sim 9°$–$10°$, and $l \sim 25°$. The different residual X-rays of the extended emission from bright X-ray sources such as low-mass X-ray binaries (e.g., GX 5−1, GX 9+1) between the All-Sky Survey and the pointed observations might cause the difference. From Figure 2*a*, it is clear that the X-ray intensity is spatially variable (reduced χ^2 about the mean $\gtrsim 5$) with a $\pm 10\%$ magnitude about the mean. A spatial Fourier transform (SFT) reveals the presence of degree-scale variations, and an $\sim 5\overset{\circ}{.}5$ scale variation is the most prominent component (Fig. 2*b*). To evaluate the significance of the SFT, a Monte Carlo test of random data drawn from a normal distribution with an average count rate of 400×10^{-6} counts s^{-1} arcmin^{-2} is performed. In this way we can evaluate how statistically improbable the calculated power of the SFT is. The probability that the observed peak in Figure 2*b* is a statistical and/or systematic fluctuation with angular scales between 2° and 10° is less than 0.1%. Intensity variation at this angular scale is also observed in each subband separately (R1L and R2), as shown in Figures 2*c* and 2*d* (R1L) and Figures 2*e* and 2*f* (R2). The detected $5\overset{\circ}{.}5$ scale variation is consistently present in the R1L band (as well as in the R2 band), which has essentially no response above 0.284 keV, indicating that the observed intensity variations are not due to "leakage" from the higher energy band ($\frac{3}{4}$ keV) emission.

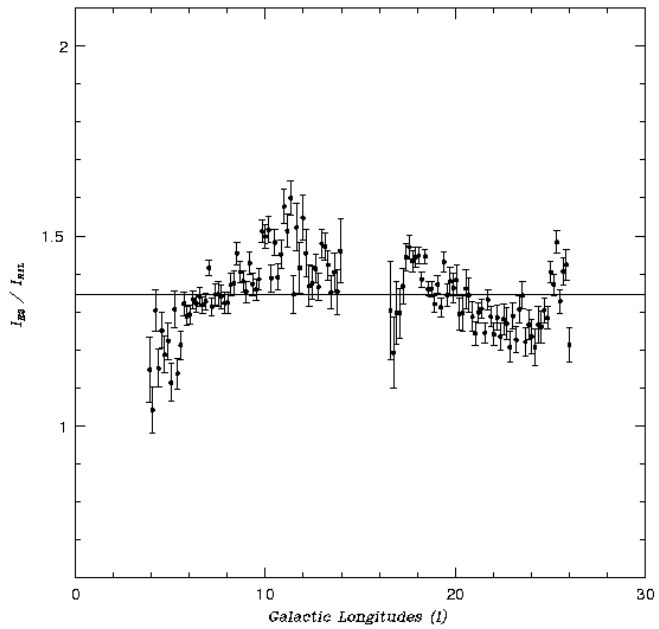

FIG. 5.—Hardness ratio of the $\frac{1}{4}$ keV band X-ray background along the Galactic plane. Each point represents the hardness ratio along the Galactic plane as integrated in 10′ columns across the Galactic plane ($b \sim -3\overset{\circ}{.}5$ to 2°). The horizontal line displays the average hardness ratio (1.35).

Sub–degree-scale variations are investigated by calculating a two-dimensional autocorrelation function (ACF) for the $\frac{1}{4}$ keV band mosaics. The following estimator of the ACF is used:

$$\mathrm{ACF}(i, j) = \frac{[N(i, j)]^{-1} \sum_{x, y, i, j} I(x, y) I(x + i, y + j)}{\bar{I}^2} - 1 ,$$

where $I(x, y)$ is the count rate in pixel (x, y), $N(i, j)$ is the number of all pixel pairs that correspond to the same scale size, $\bar{I}$ is the average count rate in all pixels that were included in the calculation at each angular scale, and (i, j) are the unit vectors for a given scale size. Pixels with poor statistics were excluded in the analysis by removing all those with an exposure less than 2000 s. This criterion excluded ~ 360 pixels ($\sim 17\%$ of the total) from the calculations.

The ACF is plotted for angular scales $\leq 3°$ in Figure 4. The ACF in both the R1L and R2 bands indicates only a slight, if any, correlation at angular scales of $\lesssim 1°$ (formal errors include zero) and none between 1° and 3°. The difference of the ACF among the three bands (R1L, R2, and R1L + R2) at this angular scale ($\lesssim 1°$) is not significant and lies within the statistical uncertainties.

The hardness ratio (I_{R2}/I_{R1L}) along the Galactic plane in the integrated 10′ bins is displayed in Figure 5. The average hardness ratio (1.35) implies a plasma temperature of $\sim 10^{6.1}$ K with no absorption. This temperature is consistent with that of the *ROSAT* All-Sky Survey (Snowden et al. 1997) for emission from the LHB.

4. DISCUSSION

The LHB is most likely interacting with the nearby Loop I superbubble, the center of which is located ~ 170 pc from the Sun. Egger & Aschenbach (1995) have shown observational evidence that the collision between the LHB and Loop I results in the formation of an annular cloud ($n_{\mathrm{H}} \sim 15$ cm^{-3}, thickness ~ 15 pc) and a "wall" ($n_{\mathrm{H}} \sim 10$ cm^{-3}, thickness ~ 3 pc) of dense neutral gas at the boundary between the two bubbles. According to the suggested

geometry, the expected neutral column density between the LHB and the Loop I superbubble is $\sim(1\text{–}7) \times 10^{20}$ cm^{-2} ($\tau \sim 1$–5 in the $\frac{1}{4}$ keV band) in the direction $4° < l < 26°$ in the Galactic plane. If the detected 5°.5 angular scale variation is due to absorption of the X-ray emission from the interior of Loop I by the intervening wall, substantial hardness ratio variations would be expected since the spectrum of Loop I is intrinsically harder than the LHB, and absorption by the boundary wall additionally hardens the observed spectrum. Our data show no evidence of such hardness ratio variations. The detected angular scale (5°.5) and magnitude ($\pm 10\%$ about the mean) of the $\frac{1}{4}$ keV X-ray intensity variations imply an emission region with a linear scale of $\lesssim 5$ pc along the line of sight. At this linear scale the neutral column density in the intervening wall is, likely, $\lesssim 3 \times 10^{20}$ cm^{-2}. Such a column density would differentially effect the R1L band more than the R2 band and cause different spatial variations between them. No significant difference in the spatial variation structure between the R1L and R2 bands is detected at angular scales $\lesssim 5°$. This leads us to assume that the contribution from the Loop I emission to the observed $\frac{1}{4}$ keV intensity is insignificant, and that *all* the observed $\frac{1}{4}$ keV flux and the detected intensity variations originate from within or at the boundary of the LHB.

The boundary shell of a supernova remnant (SNR) is generally expected to be clumpy because of Rayleigh-Taylor (R-T) instability or an inhomogeneous ambient ISM near the boundary, even if the supernova ejecta are isotropic (Lamers 1983). The observed magnitude ($\lesssim 10\%$ about the mean) and implied linear scale ($\lesssim 5$ pc at 50 pc) of the X-ray intensity variations suggest that they possibly originate as emission measure (i.e., path length) variations from such a relatively thin and clumpy boundary structure of the LHB. On the other hand, intrinsic emission variations (e.g., changes in the temperature, density, or ionization structure) at the boundary layer may also be responsible. In addition, absorbing clouds (shadowing) within the LHB cannot be completely ruled out as a possible origin.

4.1. *Magnetic Rayleigh-Taylor Instability*

Exploring possible origins of the detected X-ray intensity variations, we first consider R-T instability at the boundary of the LHB, since it has been known that a SNR in the adiabatic phase is R-T unstable at the boundary (e.g., Lamers 1983). Assuming a local cavity "reheated" by a supernova explosion, we can take an $\sim 10^5$ yr old blast wave within a very low density ($n \sim 0.004$ cm^{-3}) environment surrounding the solar system (Cox & Anderson 1982). The exact evolutionary phase of an SNR of this age ($\sim 10^5$ yr) is uncertain and could be in a "transition" between the adiabatic and radiative phases. The expected radius for the onset of the radiative stage and the amount of the swept-up mass can be estimated as a simple check for consistency with the assumed adiabatic phase. The radius for the onset of the radiative stage is given by

$$R_{\rm rad} = 24.3 E_0^{5/17} n^{-7/17} \text{ pc} ,$$

where E_0 is the initial explosion energy in units of 10^{51} ergs and n is the ambient density (cf. Plucinsky 1993). With $n = 0.004$ cm^{-3}, $R_{\rm rad}$ ranges between 120 pc (with $E_0 = 0.1 \times 10^{51}$ ergs) and 240 pc (with $E_0 = 1.0 \times 10^{51}$ ergs), which is greater than the expected LHB radius of this paper (< 100 pc; see below). The swept-up mass, $M_{\rm swept}$, is simply the ambient mass density times the LHB volume and ranges from about 30 to 270 $M_\odot$. If insufficient, these values of $R_{\rm rad}$ and $M_{\rm swept}$ are at least consistent with the adiabatic stage of SNR evolution. We also assume an average space density $n_{\rm out} = 1$ cm^{-3} outside the LHB in the Galactic plane, an electron density inside the LHB $n_e = 0.004$ cm^{-3}, and an average Galactic magnetic field $B = 5$ μG in the Galactic plane. With the given n_e and $T = 10^{6.1}$ K, the corresponding thermal pressure $p/k_{\rm B}$ is 1.0×10^4 cm^{-3} K. This gas pressure is $\gtrsim p_0/k_{\rm B} = 9000$ cm^{-3} K, a typical effective ISM pressure in the Galactic plane (Slavin & Cox 1993), and reasonably supports our assumption of an adiabatic phase for the blast wave. Although the speculated geometry of the LHB is far from spherical, in this simple model we assume a spherical geometry by adopting a reasonable range of the LHB radius, i.e., $R = 50$–100 pc in the Galactic plane with a distance of ~ 50 pc to the boundary of the LHB in this direction (Snowden et al. 1997). The stored thermal energy, $E_{\rm th}$, of the LHB has been estimated to be $\sim 3 \times 10^{50}$ ergs (Snowden et al. 1990; Cox & Anderson 1982). The thermal pressure of our model ($p/k_{\rm B} = 1.0 \times 10^4$ K cm^{-3}) yields a stored thermal energy $E_{\rm th} \sim (0.3\text{–}2.6) \times 10^{50}$ ergs, depending on the LHB radius (50–100 pc). We thus take a range of $E_{\rm th}$ of the LHB as $(0.5\text{–}3.0) \times 10^{50}$ ergs. With a typical Galactic magnetic field of 5 μG, the magnetic pressure is 1×10^{-12} ergs cm^{-3} (~ 7250 cm^{-3} K). In the adiabatic phase we can use a simple thermodynamic relation to derive the total number of particles (electrons + protons), N_P, given the thermal energy of the LHB,

$$E_{\rm th} = \int_0^R \tfrac{3}{2}\, n_P\, k_{\rm B}\, T 4\pi r^2\, dr = \tfrac{3}{2} \bar{n}_P\, k_{\rm B}\, T \tfrac{4}{3}\pi R^3 ,$$

$$N_P = \frac{2}{3}\frac{E_{\rm th}}{k_{\rm B}\, T} ,$$

where n_P is the particle density in the LHB. The estimated N_P in the LHB lies in the range $\sim(20\text{–}120) \times 10^{58}$, which is consistent with the N_P derived from the assumed emission volume and density [$\sim(12\text{–}98) \times 10^{58}$]. The "effective gravity," $g_{\rm eff}$, at the boundary of the LHB, can then be calculated with the total (thermal + magnetic) pressure, the number of protons ($\frac{1}{2}N_P$), and the emission surface area ($A_{\rm LHB}$),

$$g_{\rm eff} = \frac{(P_{\rm th} + P_{\rm mag}) A_{\rm LHB}}{(1/2) N_P\, m_p} ,$$

where $m_p = 1.67 \times 10^{-24}$ g. The range of $g_{\rm eff}$ is $\sim(0.7\text{–}16.5) \times 10^{-6}$ cm s^{-2}, depending upon the assumed size of the LHB and the stored energy. If the boundary of the LHB is magnetically R-T unstable, the mass density difference across the LHB boundary $\Delta\rho = \rho_{\rm out} - \rho_{\rm in} \sim \rho_{\rm crit} \approx \rho_{\rm out} = 2.1 \times 10^{-24}$ g cm^{-3} (given $n_{\rm out} = 1$ H I cm^{-3}; Lamers 1983), and the critical wavelength of the magnetic R-T instability, λ, can be estimated by

$$\lambda \approx \frac{B^2}{g_{\rm eff}\, \rho_{\rm out}} ,$$

assuming that the Galactic magnetic field is parallel to the boundary surface of the LHB (Jun, Norman, & Stone 1995). The estimated λ is $\sim 0.3\text{–}5.8$ pc or 0°.3–6°.6 as observed from Earth with an LHB radius of 50–100 pc (Table 2). From the comparison of the detected $\sim 5°.5$ scale variation with Table

TABLE 2

MODELED CHARACTERISTIC WAVELENGTH OF A MAGNETIC RAYLEIGH-TAYLOR INSTABILITY AT THE BOUNDARY OF THE LOCAL HOT BUBBLE

E_{th} (10^{50} ergs)	λ (pc)	Observable Angular Size (deg)
R_{LHB} = 50 pc:		
0.5	1.0	1.1
1.0	1.9	2.2
2.0	4.1	4.7
3.0	5.8	6.6
R_{LHB} = 75 pc:		
0.5	0.4	0.5
1.0	0.8	0.9
2.0	1.7	2.0
3.0	2.5	2.9
R_{LHB} = 100 pc:		
0.5	0.3	0.4
1.0	0.5	0.6
2.0	1.0	1.2
3.0	1.5	1.8

2, the magnetic R-T instability model and the data are more consistent with each other with the smaller LHB radius (50 pc), which is expected to be the case in this direction of the Galactic plane (Snowden et al. 1997).

The calculated range of angular size is remarkably consistent with the detected $\sim 5\overset{\circ}{.}5$ angular-scale X-ray intensity variations, given the inaccuracies embedded in the simple spherical adiabatic blast-wave model. The detected $\sim 5\overset{\circ}{.}5$ angular size of the X-ray intensity variation corresponds to a linear size of ~ 5 pc, for a distance of ~ 50 pc to the boundary of the LHB in this direction. It is reasonable to assume that the "amplitude" of the wavelike structure (along the line of sight) at the boundary of the LHB is comparable to the detected characteristic wavelength ($\sim 5\overset{\circ}{.}5$) of the magnetic R-T instability. Then, the detected magnitude of the X-ray intensity variations ($\pm 10\%$) is consistent with the contribution of the "extended" path length ($\lesssim 10\%$ of the assumed LHB radius) due to the amplitude of the wavelike boundary structure. In other words, the detected $\pm 10\%$ X-ray intensity variations can be associated with an $\sim 5\overset{\circ}{.}5$ "wiggling" of a magnetic R-T instability at the boundary of the LHB, superposed on the X-ray flux originating from a $10^{6.1}$ K gas that is uniformly distributed within this structure. A schematic view of the LHB boundary with the presence of a magnetic R-T instability is presented in Figure 6.

4.2. *Inhomogeneous ISM*

Another possible origin of the detected $\frac{1}{4}$ keV band X-ray intensity variations is a clumpy structure of the LHB boundary due to inhomogeneous interstellar matter near the boundary of the LHB. Even though a magnetic R-T instability at the boundary of the LHB is feasible, it is unlikely to be the case if the age of the blast wave of the LHB is $\gtrsim 10^6$ yr. The inconsistency between the adiabatic blast-wave model and the observations of the local O VI column density (Cox & Anderson 1982; Edgar 1986) may indicate that the LHB is not in the adiabatic phase. In such a case the internal and external pressures are comparable to each other and the SNR is in the radiative phase. The boundary shell may become clumpy due to inhomogeneities in the ISM (Lamers 1983).

The interstellar inhomogeneities which may cause clumps

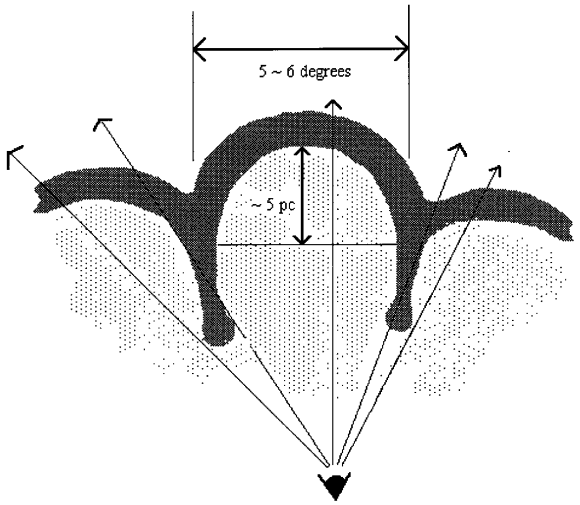

FIG. 6.—Schematic diagram of the boundary structure of the LHB with the influence of a magnetic R-T instability.

in the LHB boundary could be associated with interstellar cloudlets (Heiles 1967). The typical spatial size (2–5 pc) and internal density (1–3 cm^{-3}) of cloudlets (Heiles 1967) are consistent with the detected $\sim 5\overset{\circ}{.}5$ angular size of the X-ray intensity variations as well as the necessary additional absorption column density for the $\pm 10\%$ fluctuation. Figure 7 displays a schematic diagram for the LHB boundary structure in the radiative phase.

4.3. *Emission Variations at the Boundary Layer*

The observed intensity variations may also originate from emission variations at the LHB boundary. While the X-ray–emitting gas inside of the LHB is most likely uniformly distributed, temperature and/or density fluctuations are probably present at the boundary layer. These fluctuations can cause emission variations from the LHB boundary. Recent measurements utilizing scintillation from nearby pulsars have revealed density fluctuations near the LHB boundary layer. Phillips & Clegg (1992) found that derived electron density variations can be up to an order of magnitude lower than the local mean electron density. Such electron density variations at the LHB boundary could

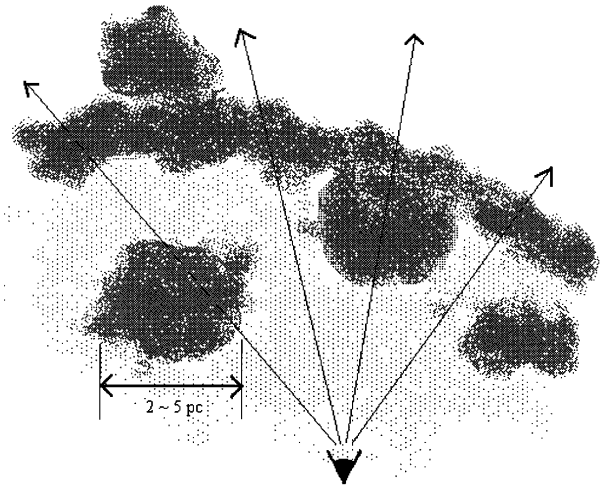

FIG. 7.—Schematic diagram of the boundary structure of the LHB with the presence of inhomogeneous ISM (e.g., roughly parsec-scale cloudlets) near the boundary shell.

induce significant emission variations that are detectable in soft X-rays. For detailed characteristics of the possible emission variations sufficient to produce quantitative predictions, particularly at low Galactic latitudes, more extensive studies need to be performed.

4.4. *The Local Fluff and Embedded Clouds*

The column density of the "Local Fluff" is $\lesssim 3 \times 10^{18}$ cm^{-2} (Frisch 1995) and is too low to produce the observed $\pm 10\%$ X-ray intensity variations in the $\frac{1}{4}$ keV band ($N_{\rm H} \gtrsim 10^{19}$ cm^{-2} is required). The Local Fluff therefore is not the source of the detected $\pm 10\%$ scale X-ray intensity variations.

The observed variation could also be produced as an absorption effect by clouds within the LHB. For a cloud halfway through the LHB to produce a 20% drop in the observed flux, the transmission must be 60%. The clouds must therefore have a column density of $\sim 5 \times 10^{19}$ cm^{-2}. Assuming that the clouds are spherical with a 5° diameter and are at a distance of 25 pc, this implies a space density of $n_{\rm H} \sim 7$ cm^{-3} and a total mass of about 1 $M_\odot$. Recent observations have revealed the presence of local interstellar clouds with $n = 0.1$–1 cm^{-3} within ~ 100 pc, for instance, the dense H I filament with $N_{\rm H} \sim 8 \times 10^{19}$ cm^{-2}, $n_{\rm H} \sim 75$ cm^{-3}, and $d \lesssim 60$ pc, detected by Kerp, Herbstmeier, & Mebold (1993).

5. SUMMARY AND CONCLUSIONS

Mosaics of the 42 *ROSAT* PSPC pointed observations were used to search the $\frac{1}{4}$ keV band soft X-ray background for intensity variations at various angular scales along the Galactic plane ($l \sim 4°$–$26°$). Degree-scale X-ray intensity variations were detected and the magnitude of the intensity variations is $\pm 10\%$ about the mean. The interpretation of the results strongly depends on adopted assumptions such as the age of the blast wave, stored energy in the LHB, and the exact geometry and size of the LHB. With a simple model of a reheated spherical blast wave ($\sim 10^5$ yr old) in the adiabatic phase within a preexisting local cavity, the detected $\sim 5\overset{\circ}{.}5$ scale angular variations with $\pm 10\%$ magnitude in the $\frac{1}{4}$ keV band X-ray background can be described in terms of a magnetic Rayleigh-Taylor instability at the boundary of the LHB. If the blast wave is older than 10^6 yr, the SNR is probably in the radiative phase, and a Rayleigh-Taylor instability is unlikely. Alternatively, the X-ray intensity variations then should be more sensitive to inhomogeneities in the ISM such as the existence of interstellar cloudlets. The typical characteristics of interstellar cloudlets may produce the observed $5\overset{\circ}{.}5$ scale X-ray intensity variations. Emission variations at the LHB boundary layer may also exist and cause the detected X-ray intensity variations. While absorption by interstellar clouds within the LHB may not be ruled out, because of its low density, the LF cannot produce the observed $\pm 10\%$ intensity variations at $5\overset{\circ}{.}5$ angular scale.

The smoothness of the observed $\frac{1}{4}$ keV background can be used to argue against models for its origin that suggest an extensive intermixture of emitting and absorbing gas, similar to the McKee & Ostriker (1977) picture of the ISM. Such models embed the cooler material of the Galactic disk as separate, relatively compact clouds in a matrix of hot gas. If such is the case, the individual clouds must have column densities of low optical depth ($\lesssim$ a few $\times 10^{19}$ H cm^{-2}) so as not to produce significant absorption features. Since the region of the mosaic lies in the direction of the interior of the nearby Loop I SNR/stellar wind bubble, which is a bright background source of diffuse X-rays separated from the LHB by less than a few tens of parsecs, the smoothness and lack of strong hardness variations imply a rather continuous intervening wall or sheet of H I. Any hardness variations due to variable absorption of the Loop I emission by the intervening wall, if the transmitted flux is significant, should be extreme, as the intrinsic emission is harder than that in the LHB and absorption only serves to further harden the spectrum.

The authors would like to thank K. Kuntz for his extensive help with the autocorrelation function analysis. We also thank R. Egger for useful discussion regarding the Local Hot Bubble–Loop I superbubble interaction model. This research has made use of data obtained through the High Energy Astrophysics Science Archive Research Center Online Service, provided by the NASA Goddard Space Flight Center and was supported in part by NASA grants NAG 5-2492, NAG 5-3426, and the Purdue Research Foundation.

REFERENCES

Bloch, J. J., Jahoda, K., Juda, M., McCammon, D., Sanders, W. T., & Snowden, S. L. 1986, ApJ, 308, L59
Bowyer, C. S., Field, G. B., & Mack, J. E. 1968, Nature, 217, 32
Cox, D. P., & Anderson, P. R. 1982, ApJ, 253, 268
Cox, D. P., & Reynolds, R. J. 1987, ARA&A, 25, 303
Edgar, R. J. 1986, ApJ, 308, 389
Egger, R. J., & Aschenbach, B. 1995, A&A, 294, L25
Frisch, P. C. 1995, Space Sci. Rev., 72, 499
Frisch, P. C., & York, D. G. 1983, ApJ, 271, L59
Heiles, C. 1967, ApJS, 15, 97
Juda, M., Bloch, J. J., Edwards, B. C., McCammon, D., Sanders, W. T., Snowden, S. L., & Zhang, J. 1991, ApJ, 367, 182
Jun, B.-I., Norman, M. L., & Stone, J. M. 1995, ApJ, 453, 332
Kerp, J., Herbstmeier, U., & Mebold, U. 1993, A&A, 268, L21
Knapp, G. R. 1975, AJ, 80, 111
Lamers, H. J. G. L. M. 1983, in Diffuse Matter in Galaxies, ed. J. Audouze, J. Lequeux, M. Lévy, & A. Vidal-Madjar (NATO ASI Ser. C, 110) (Dordrecht: Reidel), 45
McCammon, D., Burrows, D. N., Sanders, W. T., & Kraushaar, W. L. 1983, ApJ, 269, 107
McCammon, D., & Sanders, W. T. 1990, ARA&A, 28, 657
McKee, C. F., & Ostriker, J. P. 1977, ApJ, 218, 148
Paresce, F. 1984, AJ, 89, 1022
Phillips, J. A., & Clegg, A. W. 1992, Nature, 360, 137
Plucinsky, P. P. 1993, Ph.D. thesis, Univ. Wisconsin, Madison
Sanders, W. T., Kraushaar, W. L., Nousek, J. A., & Fried, P. M. 1977, ApJ, 217, L87
Slavin, J. D., & Cox, D. P. 1992, ApJ, 392, 131
———. 1993, ApJ, 417, 187
Snowden, S. L., Cox, D. P., McCammon, D., & Sanders, W. T. 1990, ApJ, 354, 211
Snowden, S. L., Egger, R., Finkbeiner, D., Freyberg, M. J., McCammon, D., Plucinsky, P. P., & Sanders, W. T. 1997, ApJ, submitted
Snowden, S. L., et al. 1995, ApJ, 454, 643
Snowden, S. L., McCammon, D., Burrows, D. N., & Mendenhall, J. A. 1994, ApJ, 424, 714
Williamson, F. O., Sanders, W. T., Kraushaar, W. L., McCammon, D., Borken, R., & Bunner, A. N. 1974, ApJ, 193, L133